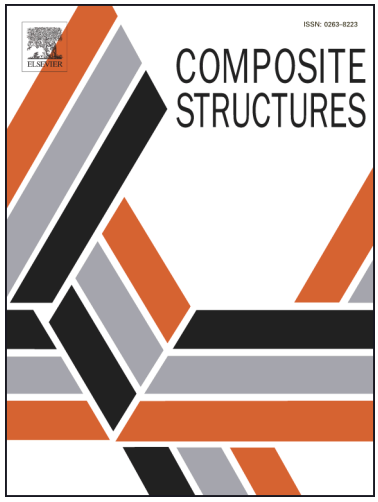

Structural behavior of a lightweight, textile-reinforced concrete barrel vault shell

E. Sharei, A. Scholzen, J. Hegger, R. Chudoba

PII: S0263-8223(17)30394-X
DOI: http://dx.doi.org/10.1016/j.compstruct.2017.03.069
Reference: COST 8390

To appear in: *Composite Structures*

Please cite this article as: Sharei, E., Scholzen, A., Hegger, J., Chudoba, R., Structural behavior of a lightweight, textile-reinforced concrete barrel vault shell, *Composite Structures* (2017), doi: http://dx.doi.org/10.1016/j.compstruct.2017.03.069

Structural behavior of a lightweight, textile-reinforced concrete barrel vault shell

E.Sharei

Institute of Structural Concrete, RWTH Aachen University, Germany,
tel: +49 241 8025172, fax: +49 241 8022335, e-mail: esharei@imb.rwth-aachen.de

A.Scholzen, J.Hegger, R.Chudoba

Institute of Structural Concrete, RWTH Aachen University, Germany

Abstract

Textile-reinforced concrete (TRC) as a novel composite material offers a wide range of capabilities and flexibility in the manufacturing of thin-walled, lightweight structures. The application of textile reinforcement in fine aggregate high-performance concrete has enabled the dimensioning of structural concrete in very small thicknesses. This possibility allows for the fabrication of thin-walled TRC shell structures with complex geometries. On the other hand, structural planning and construction require new modeling approaches to comprehend the structural behavior of such forms. In this paper, we present the fabrication procedure of a large-scale TRC vault shell, together with the performed experimental study. The shell structure was tested under a two-step loading scenario to study the load-bearing behavior. The particular focus of the paper is on the analysis of the structural behavior by means of an anisotropic strain-hardening material model specifically developed for the simulation of TRC shells. The prediction obtained using the nonlinear finite element simulation has been compared with the test results to validate the modeling approach. The performed studies are used to evaluate and discuss the structural redundancy included in the applied linear ultimate limit state assessment procedure.

Keywords: Textile reinforced concrete, Carbon concrete, Thin-walled shells, Cementitious composites, Composite structures, Finite Element Analysis, Microplane damage model

1. Introduction

The design and construction of thin-walled shells made of cementitious composites for use in architecture and civil engineering bring about several challenging questions that span the fields of material development, production technology, and safety assessment. The combination of high-performance carbon or glass textile fabrics with a fine-grained cementitious matrix opens up new possibilities for the design of lightweight structures with high degree of material utilization. Because of the flexibility in shape and resistance to corrosion of the textile fabrics, thin concrete shells with shapes tailored to specific boundary conditions can be produced that would not be feasible using traditional steel reinforcement.

Textile-reinforced shells recently constructed at the campus of the RWTH Aachen University were motivated by the need to illuminate the potential of the novel composite material and, at the same time, to examine the suitability of the developed design and production methods for engineering practice. In particular, the manufacturing aspects involved in the construction of the hypar shells serving as roof of the T3 Pavilion [1] were addressed in detail in [2]. The methods applied to characterize the material, including the experimental procedures and structural performance assessment, were described by the authors in [3]. Another carbon concrete shell with a barrel vault shape serving as a roof element over a bicycle stand (Fig. 1) was recently presented in [4, 5] with a focus on the formulated procedure of ultimate limit state assessment.

Reliable dimensioning and assessment rules for a wide range of TRC shell applications can only be formulated with an in-depth understanding of all relevant aspects of their structural behavior. The required insight into the correspondence between the composite material structure, shell shapes, boundary conditions, possible stress redistribution mechanisms, and failure scenarios can be gained using advanced numerical models reflecting specific aspects of the TRC structural shell behavior. We consider the following three phenomena in the material and structural behavior, which are essential for the formulation of a realistic modeling framework to serve as the basis of future code standards and design tools:

- The tensile response of a shell cross section exhibiting strain-hardening effect owing to an evolving fine crack pattern.
- Two-dimensional anisotropic damage owing to matrix cracking and debonding within a shell cross section exposed to combined normal and bending loading.

(a) (b)

Figure 1: (a) TRC barrel vault shells as roof elements; (b) bicycle stand consisting of five singly curved shells.

- Buckling and stability behavior in response to compressive stresses within a thin-walled shell structure.

In order to set the present work within the broader context of existing modeling approaches, we will shortly review recent developments in the field of numerical modeling and experimental observations in relation to the three aforementioned phenomena in the following subsections.

(I) Uniaxial tensile behavior. Based on the need to understand and characterize the tensile behavior of quasi-ductile composites, several modeling approaches have been developed in recent years with the intention of reflecting the elementary damage mechanisms of matrix cracking and the debonding of the fabric from the matrix. Mesoscale models with explicit representation of the reinforcement layout within the cross section enable the study and understanding of the damage evolution process in the composite, and can be used to identify suitable combinations of materials, fabric geometries, short fiber volume fractions, and lengths [6, 7, 8, 9, 10]. Special attention has been paid to the modeling of the local disintegration process within the inherently heterogeneous bond structure in cementitious composites reinforced with multi-filament yarns in the crack bridge and its vicinity [11].

Experimental studies of cementitious composites reinforced with textile fabrics or with short fibers have also been reported (e.g., in [12, 13]). Experimental research on the tensile behavior of textile-reinforced concrete has been presented in [14, 15, 16]. A standardized tensile test setup for textile-reinforced concrete has been recently published in a RILEM recommendation [17].

(II) Two-dimensional, anisotropic damage propagation. Modeling approaches reflecting the interaction between the matrix and reinforcement within a thin plate in a finite element model have been presented by several authors [18, 19]. These models describe the bond between fabrics and matrix as a two-dimensional, zero-thickness interface with slip displacement governed by a predefined bond law. These approaches are suitable for sparsely reinforced cross sections with one or two reinforcement layers. Another example of this modeling approach was presented in [20], in which two bond interfaces were used: one between the concrete matrix and sleeve filament, and the other between the sleeve and core filaments. The model considers a nonlinear elasto-plastic material model for the concrete matrix, and an idealized linear elastic behavior with tension stiffening for the fabric reinforcement.

The modeling approach followed in this paper uses a smeared representation of the material structure within a cross section, describing the cracking and debonding phenomenologically in terms of an anisotropic damage tensor. Such an idealization assumes a homogeneous layout of reinforcements over the cross-sectional height. The applied numerical representation of a cross section is sketched in Fig. 2, indicating the types of cross sections that can be addressed by the smeared modeling approach; namely, cementitious composites with randomly distributed short fibers (i), regularly distributed, continuous fabrics (ii), or combinations of both (iii). It is possible to reflect both strain-softening and strain-hardening composites using dispersed, finely distributed reinforcements.

The numerical idealization described here is related to approaches for modeling ordinary steel-reinforced concrete shells developed in recent decades [21, 22]. The modeling approaches were developed for the simulation of large-scale shell structures, such as cooling towers or power plants. In these structures, the development of a crack pattern with very small crack distances compared to the size of the structure justifies a smeared approach to model the material behavior at the level of a shell cross section. Examples of finite element shell formulations combined with an elasto-plastic damage model to simulate reinforced concrete shells under monotonic and cyclic loads have been presented in [23], employing a Drucker-Prager type elasto-plastic damage model in compression and a continuum damage model with a Rankine stress limit in tension. Using the same material model, the damage evolution and

failure of large cooling towers was investigated in [24], considering a two-dimensional failure mode within the shell elements. In another numerical framework for the nonlinear analysis of the damage evolution in steel-reinforced concrete shells, three major topics that may affect the accuracy of the simulations were covered: (1) the formulation of adequate finite elements to describe the shell geometry, as well as the boundary and load conditions; (2) the development of realistic material models; and (3) the estimation of discretization errors [25].

The modeling methods described provide valuable insight for the formulation of design models that realistically reflect the ultimate limit state assessment of shell structures. Examples of design tools developed were provided, for example, in [26], which describes a framework for the integrated design, analysis, and assessment of the load-bearing capacity of segmented concrete shell structures. The development of numerical techniques in the coupled analysis of the manufacturing process and anisotropic material behavior of fiber-reinforced polymer thin-walled shells was presented in [27]. Meanwhile, the safety and reliability analysis of reinforced concrete shells is presented in [28], using response surface methods and axisymmetric nonlinear finite element analysis. An example of a design model for the prediction of the moment-curvature relationship of a TRC cross section has been presented in [29], which derives design equations and charts for flexural composite members. The general framework for dimensioning and assessing thin-walled, regularly reinforced TRC shells reflecting the two-dimensional interaction between normal forces and bending moments has been presented by the authors of[4]. The application of this design model to a large-scale pavilion with a TRC roof has been described in [2].

(III) Compressive stresses and stability. Numerical analysis of the buckling and stability of steel-RC shells that considers their nonlinear material behavior through a work-hardening plasticity model with the Drucker-Prager yield criterion has been presented in [30]. The numerical model was used to study the structural response of cooling tower shells with the compressive biaxial behavior of concrete. Further modeling aspects, such as the influence of creep on the buckling behavior of reinforced concrete shells, were presented in [31].

The applicability of textile-reinforced concrete in the construction of shell structures with a focus on their buckling behavior and stability was investigated in [32]. The effect of geometric imperfections on the buckling capacity of funicular and dome shells has been studied in [33, 34, 35, 36]. These studies were performed using a linear elastic material model. In a recent paper, the effect of geometric imperfections on the structural behavior of the present TRC vault shell considering geometrical nonlinearity has been studied by the authors in [37]. This study evaluated the sensitivity of structural behavior under compression with respect to the interaction of

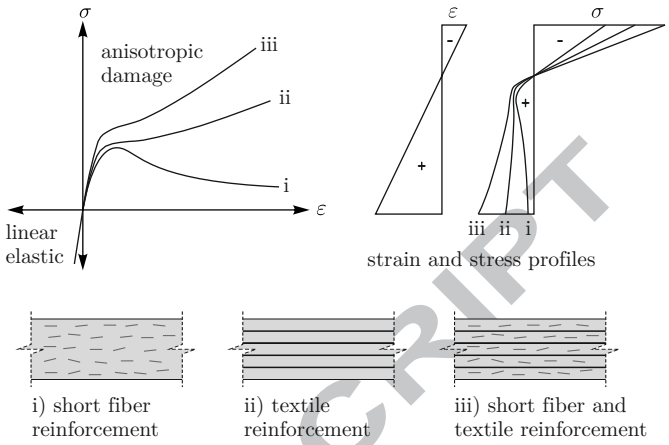

Figure 2: Tensile and compressive behavior of idealized cross sections for application to smeared modeling of strain softening and strain hardening cementitious composites

the anisotropic strain-hardening behavior and geometric imperfections.

In the present paper, we focus primarily on the first two aspects of the structural behavior described above, with the intention of documenting the validity of the model and providing a detailed interpretation of the full-scale test that has been performed. The effect of geometric imperfections is not studied here, as it proved to be insignificant in the case of the tested shell. The paper is organized as follows: In Sections 2 and 3, we briefly explain the material model and its calibration for the cross section of the barrel vault shell. Section 4 describes the dimensioning and fabrication of the shell structure and the performed full-scale test. Then, in Section 5, we present the simulation procedure and the numerical results, and assess the validity of the model by comparing the prediction with the test results. Finally, Section 6 presents the ultimate limit state assessment of the barrel vault shell, based on linear elastic analysis.

2. Modeling approach

In a recent paper [38], the authors have presented a smeared modeling approach to the simulation of TRC shells based on the microplane damage model, originally introduced by Jirásek [39] for strain-softening materials. The damage-based, anisotropic material model was utilized and extended to comply with the kinematics of thin shells with anisotropic strain-hardening behavior. In addition, geometric nonlinearity has been considered to reflect the effect of large *out-of-plane* deflections on the membrane forces. At the same time, a systematic calibration procedure using uniaxial tensile tests to determine the material parameters of a particular TRC cross section has been proposed. The capability of the model to capture the nonlinear material behavior was validated through the simulation of a slab test. The proposed modeling approach

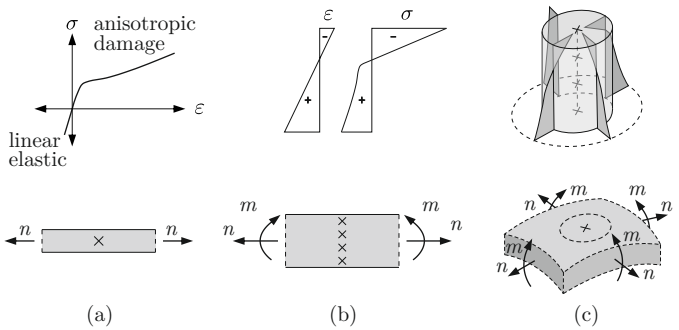

Figure 3: Anisotropic approach to the modeling of strain hardening shells (a) uniaxial behavior; (b) stress/strain state along the thickness for the interaction of bending and tension; (c): *in-plane* stress state for a shell segment

has been used to study selected aspects of the structural behavior of TRC shells in [40].

The idealization of the material behavior used in the present formulation is summarized in Fig. 2. The strain-hardening tensile response is shown at the level of a single integration point (Fig. 3a). The behavior of a cross section exposed to combined tension and bending action is reflected by using the assumption of linear strains over the cross-sectional height and integrating the stress over an adequate number of integration points (Fig. 3b). The two-dimensional, anisotropic *in-plane* stress-strain response due to the formation of cracks [41](Fig. 3c) is accounted for by using the polar representation of the *in-plane* strain and stress states of a shell cross section. This type of idealization is appropriate for cross sections with fine crack pattern developing under tensile loading, which can be represented as smeared anisotropic damage. This was the case in the present vault shell.

2.1. Description of the material model

Material models formulated using the microplane approach define constitutive relations between the strain and stress at the level of an oriented plane, called *microplanes* [42]. The damage evolution of a microplane is governed by a damage function. The shape of the damage function can be tailored for either quasi-brittle materials with strain-softening behavior, e.g. plain concrete [39], or it can reproduce the strain-hardening behavior of quasi-ductile materials, such as TRC [38].

The basic structure of a microplane model is shown in Fig. 4a. The anisotropic strain-stress mapping is not formulated directly between stress and strain tensors, but indirectly in three steps, as shown in Fig. 4b: (i) geometric projection of the macroscopic strain tensor $\boldsymbol{\varepsilon}$ onto the microplane directions, providing strain vectors $\boldsymbol{e}$; (ii) application of the constitutive damage law between strain vector $\boldsymbol{e}$ and stress vector $\boldsymbol{s}$; and (iii) energetic homogenization of microplane stress vectors based on the principle of virtual

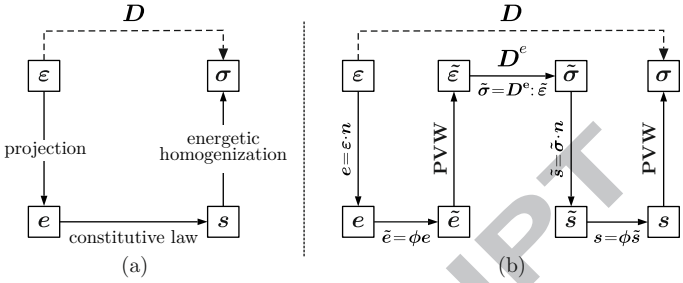

Figure 4: (a) basic principle of microplane model; (b) constitutive stress-strain relation in microplane damage model

work (PVW) to obtain the stress tensor $\boldsymbol{\sigma}$. In this formulation, the mapping of apparent strain/stress vectors ($\boldsymbol{e}$ and $\boldsymbol{s}$) to the effective strain/stress vectors ($\tilde{\boldsymbol{e}}$ and $\tilde{\boldsymbol{s}}$) is done at the microplane level using a damage function $\boldsymbol{\phi}\,(\boldsymbol{e_{max}})$. The principle of virtual work enforces the equality of the virtual work at the microscopic and macroscopic levels. A salient feature of this microplane formulation is the explicit representation of elastic stiffness tensor $\boldsymbol{D^e}$, which links the effective strains $\tilde{\boldsymbol{\varepsilon}}$ and stresses $\tilde{\boldsymbol{\sigma}}$ of an undamaged material skeleton. For a complete description of the material formulation and calibration procedure, we refer to the related paper [38].

The material model presented here has been implemented in a finite element code for five-parameter shell elements. In this shell formulation, a two-dimensional formulation of the microplane damage model with strain-hardening for TRC was used in the *in-plane* direction. Linear elastic behavior was assumed in the *out-of-plane* direction.

3. Calibration procedure

The damage function $\boldsymbol{\phi}\,(\boldsymbol{e_{max}})$ determines the loss of integrity at the level of a material point. It is prescribed as a function of the maximum microplane strain achieved over the loading history $\boldsymbol{e_{max}}$. The damage function of a particular TRC cross section can be obtained by using an experimentally measured tensile stress-strain response of the corresponding TRC specimen through applying an incremental inverse analysis, as described in [38].

The TRC cross section considered for the production of the bicycle shelter consisted of six layers of non-impregnated, wrap-knitted carbon textile fabric (Fig. 5a). The carbon textile fabric was produced as orthogonal grids with equidistant spacings between rovings in both directions. The shells were manufactured through the successive application of the reinforcement and of the shotcrete layers into the formwork [5]. A series of tensile tests was performed on TRC specimens (Fig. 5b) with the given cross section to provide the stress-strain curves as targets for the calibration procedure. Cross-sectional properties of the utilized TRC specimens and their dimensions are summarized in Table 1.

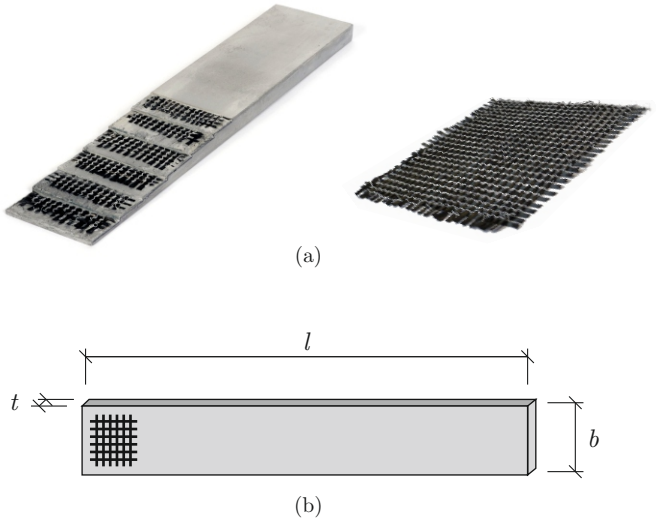

Figure 5: (a) cross-sectional layout of TRC vault shell containing 6 layers of nonimpregnated carbon fabrics; (b) tensile test specimen

Table 1: Properties of the TRC cross section

Description	Symbol	Value	Unit
width	b	100	mm
thickness	t	20	mm
length	l	1000	mm
total cross section	A	2000	mm^2
number of textile layers	n_{tex}	6	—
layer distance	s_{tex}	2.9	mm
concrete cover	c	2.9	mm
yarn spacing	s_{yarn}	8.3	mm
yarn cross section	A_{yarn}	0.446	mm^2
textile cross section	A_{tex}	32.1	mm^2
reinforcement ratio	ρ_{tex}	1.61	% by vol.

The stress-strain curve measured in the tensile test is plotted with a gray, dashed line in Fig. 6a. By setting this curve as the target in the calibration algorithm, the damage function in Fig. 6b was calibrated using the procedure described in [38] with a modulus of elasticity of the concrete matrix $E_{\text{c}} = 18.7$ GPa and Poisson's ratio $\nu = 0.2$. The simulation of the tensile test using a single material point represents the stress-strain curve of the tensile test, depicted with a solid line in Fig. 6a.

4. Large-scale test on a TRC vault shell

4.1. Shell design and fabrication

The experimental study of the structural response of the TRC shells depicted in Fig. 1b was performed within an applied research project focused on the examination and

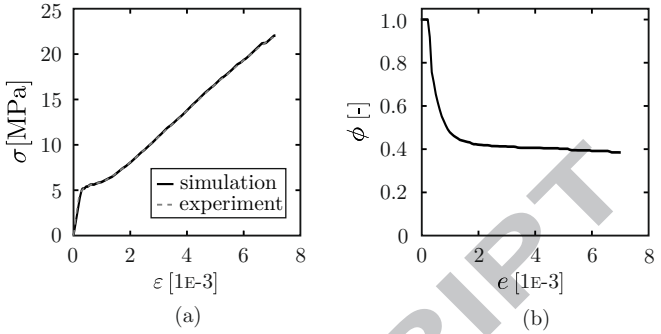

Figure 6: (a) stress-strain curve of the tensile test; (b) calibrated damage function

verification of the developed design, manufacturing, and construction methods for TRC on a real-world structure.

The side view of the shell and the corresponding section A-A at the supports are shown in Fig. 7, with related dimensions. The shells have a maximum length of 4.40 m in the x-direction and a width of 2.14 m in the y-direction, providing a total roofing area of 48 m^2. The weight of the 20 mm thick shell is about 420 kg. The shell section is represented by a segment of a cylinder with an inner radius of 1.38 m, providing an opening angle of 100.2°. In the x-direction, the shell is supported by two steel angles on each side at a distance of 2.6 m from each other. The supports provide adjustable constraints in the r-direction through screwed plates, and fixed constraints in the θ-direction (Fig. 7 right). In order to avoid direct contact between the shell and steel supports, elastomer layers were used in both the radial and tangential directions.

The cross-sectional thickness and reinforcement layout of the shell were the same as those for the tensile tests used to calibrate the model, as described in Section 3. Due to the need for high form-flexibility of the fabric, non-impregnated textile fabrics were used.

4.2. Test setup, boundary conditions and loading history

The test setup was designed with the goal of demonstrating the high ductility of the structure, stemming from the interplay between the strain-hardening material behavior and the stress redistribution over large zones of the shell. Therefore, it was important to avoid local failure. In particular, high local bending moments or local shear failure near the supports were undesirable, as they would induce early failure without sufficient information about the overall structural behavior.

Keeping these considerations in mind, the test setup has been designed as follows: the shell was supported at four points located near the corners, consistent with the actual structural design depicted in Fig. 1. In order to avoid a local stress concentration, a thin metal sheet strip with cross-sectional dimensions of $w/h = 6/80$ mm was laid along the y-direction over the middle section of the shell, as depicted in Fig. 8b, and connected to hydraulic cylinders fixed to the ground at an angle of 38°, as shown in Fig. 8c.

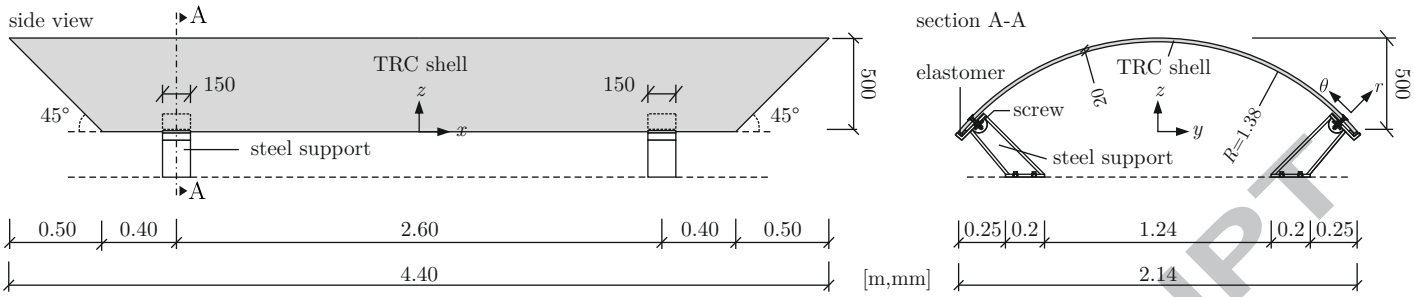

Figure 7: Dimensions of the TRC roof element in side view and section

This kind of loading device induces smooth stress gradients within the shell without local stress peaks. Two additional greased steel sheets were laid in between the metal sheet and the shell surface to minimize friction. Using this load device, the tension load S introduced by the hydraulic cylinders was transformed into a constant, radial line load q in the middle section of the shell, as indicated at the top of Fig. 9 following the analytical formula $q = S/R$ with $R = 1.38$ m denoting the vault radius.

The load S was applied in two steps with changing support configurations, as depicted in Fig. 9. In the load step I, radial displacements in the r-direction at the supports were set free, as shown in Fig. 9a, with the intention to induce the widespread distribution of fine cracks over a large zone of the shell. The load S was increased to 60 kN (t_1). After that, the system was unloaded. Then, the radial displacements at the supports were fixed, as depicted in Fig. 9b, and the shell was reloaded up to the failure load of 98.4 kN (t_2).

During the test, shell deformations were recorded by measuring the tensile strains ε_{xx} in the expected failure crack regions, at the midspan of the edges in the x-direction. As shown in Fig. 8a, the 300 mm long displacement gauges were placed along the shell edges at these positions. The gauge length was the same as for the tensile test shown in Fig. 6 to have the comparable measure of strain during the test. In this way, the maximum strain measured during the test served as an indicator of the approaching ultimate failure of the shell. Also, the vertical deflections w_z at points P_1 to P_7 located on the top of the shell along the x-direction were measured using vertical displacement gauges, as shown in Fig. 8a.

5. Finite element simulation of TRC vault shell

The finite element discretization was performed using bilinear quadrilateral five-parameter shell elements with three translational and two rotational degrees of freedom at each node. In the applied *ABAQUS* code, this element is referred to as a *conventional* shell element [43]. The finite element mesh was generated by mapping a regular grid of 30×40 onto the shell surface. The mesh size varies in the range of $85 \sim 110$ mm in the x-direction and $70 \sim 105$ mm in the θ-direction.

The steel strip used to apply the load S was modeled using the same element type as that used for the TRC shell. A linear elastic material model with a modulus of elasticity of $E_s = 210$ GPa and a Poisson's ratio of $\nu = 0.3$ was used for steel. The interaction between the steel strip and the TRC shell was defined by frictionless contact. The boundary conditions of the shell were defined corresponding to the two-step loading history described in Section 4.2. By defining local coordinate systems at support positions, the degrees of freedom in the r- and θ-directions were constrained depending on the load step. As shown in Fig. 9, during load step I, only the constraints R_θ in the θ-direction were active, providing degrees of freedom in the r-direction. After unloading the system, the radial constraints R_r at the supports (caused by screws in the r-direction) were added, and the system was loaded further in load step II.

The compressive deformation of the elastomers δ and the reaction force at the supports R_θ were measured during the test. The corresponding load-deformation curves are plotted with gray dashed lines in Fig. 9d. In order to reflect the compliance of the elastomer in the numerical model, linear springs connected to the steel supports were used with a stiffness of $k = R_\theta/\delta_{\max} \approx 14000$ kN/m, indicated with a solid line in Fig. 9d.

The deformed configuration of the TRC vault shell and the propagation of damage at the end of load step II are shown in Fig. 10a. In this figure, the parameter $\omega = 1 - \max(\phi)$ describes the maximum level of microplane damage in each material point of the shell. As desired, the test setup induces a widespread distribution of damage, observed as finely distributed cracks in the test (Fig. 10c). The failure crack appeared in the middle section of the shell edge (Fig. 10b). The distribution of the damage corresponded well with the observed crack pattern, with crack distances ranging between $5 \sim 10$ mm (see Fig. 10a).

The structural behavior of the shell is well-documented through the diagram linking the load S to the strain evolution at the failure zone, as shown in Fig. 11. The average tensile strain ε_{xx} was measured within the length of 300 mm, using two horizontal displacement gauges at the front and back edges of the shell. Correspondingly, ε_{xx} was evaluated similarly in the numerical model. The measured curves are plotted with gray dashed lines, while the

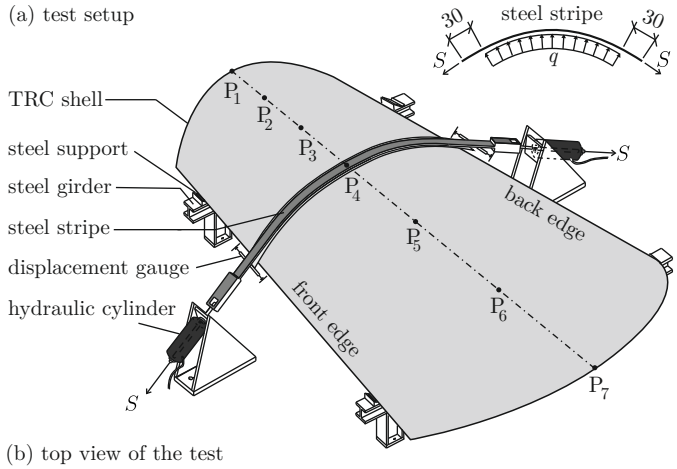

(b) top view of the test

(c) hydraulic cylinder

Figure 8: (a) test setup of the TRC vault shell with corresponding support conditions, loads and measuring points ; (b) test specimen in the laboratory and (c) detail of the hydraulic cylinder for the application of load S (bottom)

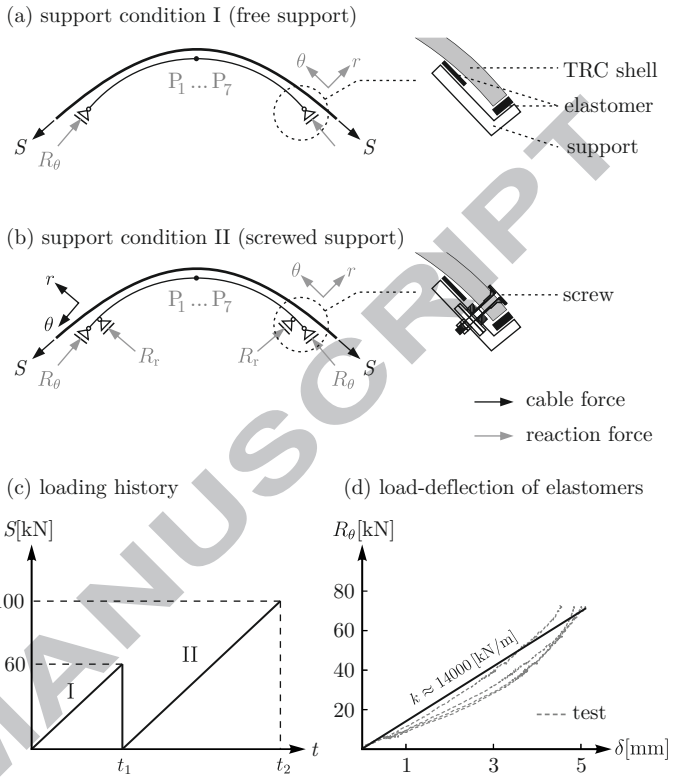

Figure 9: (a) free support conditions at loading step I; (b) screwed support conditions at loading step II; (c) time history of load S; (d) estimation of stiffness of elastomers k using the measured load-deflection curves at supports

simulation results are shown with solid lines. The effect of the changed boundary conditions due to the fixed radial component of the supports could be reproduced well through the numerical model. In general, the simulated predictions are in good agreement with the test response. Due to the fact that the shell was not perfectly symmetric, the strains measured along the front edge turned out to be slightly smaller (Fig 11 top).

Let us emphasize, that in the present form, the model describes the nonlinear material behavior purely as damage. The dissipative terms associated with plastic deformation are not explicitly distinguished. As a consequence, the simulation can only reflect the anisotropic redistribution of stresses owing to damage propagation for increasing loading. Thus, the comparison between the test and simulation is limited to the ascending loading branches, the unloading branch cannot be reproduced. In a damage-based model, unloading to zero load induces zero strains while preserving the damage state in the structure achieved at the end of the first loading branch. It would certainly be valuable to present also the unloading branch of the test to show the amount of permanent deformation in the composite after unloading. Unfortunately, this data is not available due to a malfunction of the measuring equipment that occurred during the unloading process.

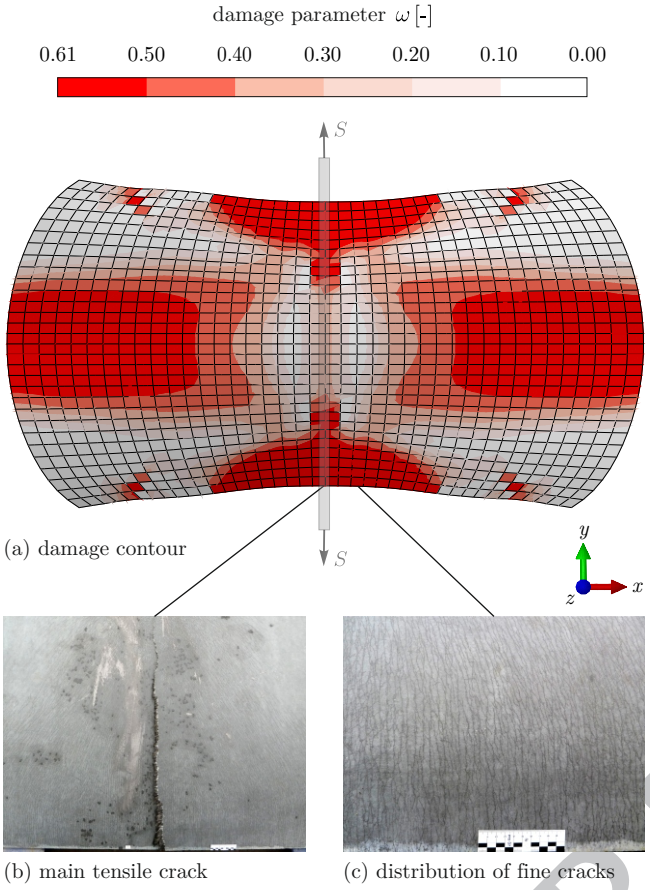

(a) damage contour

(b) main tensile crack

(c) distribution of fine cracks

Figure 10: (a) damage plot of the TRC vault shell in deformed configuration at the end of load step II; (b) tensile rupture at mid-span; (c) distribution of multiple fine cracks

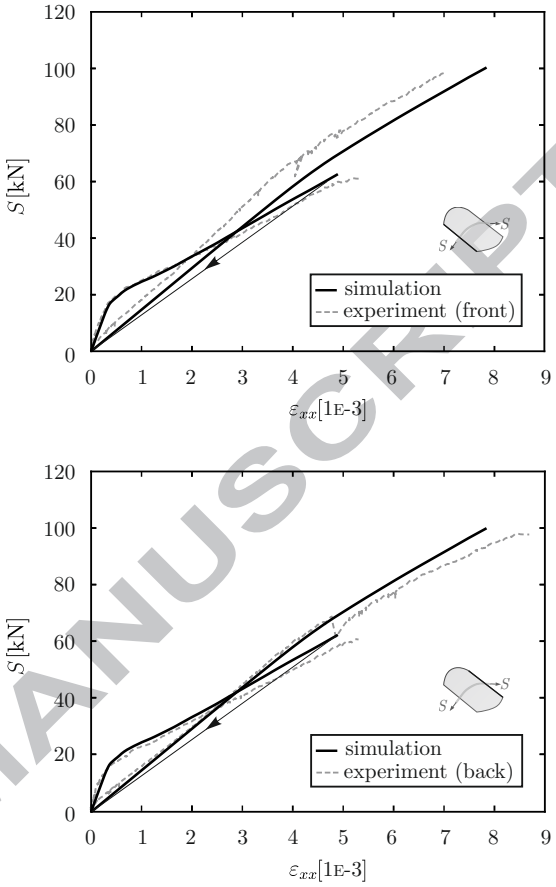

Figure 11: Load-strain curves from test and simulation in the tensile region of the TRC vault shell for the front edge (top) and back edge (bottom) in x-direction

In can only be concluded from the horizontal shift between the loading branches, that the permanent deformation achieved in the critical cross section was in the range of $1\text{E}{-3} < \varepsilon_{xx,\text{p}} < 2\text{E}{-3}$.

Even without considering the permanent deformation after the first loading branch, the maximum tensile strain $\varepsilon_{xx,\text{u}} = 8.6\text{E}{-3}$ in the critical cross section was higher than the mean value $\varepsilon_{xx,\text{u}} = 7.6\text{E}{-3}$ obtained in the tensile tests. This can be explained by a smoother stress field gradient along the shell edge, compared to the situation in the tensile test with inherently steep stress gradients in the clamped area of the specimen [4]. Another reason for higher effective tensile strength within the shell could be the simultaneous action of bending and tension, as discussed in detail by the authors in [37, 44].

The evolution of damage during the loading history is shown in Figs. 12 for three stages during load steps I and II. For step I, with the radial component of the displacement supports released, crack evolution could be observed starting at the mid-span of the longitudinal edges and at both curved edges, propagating into the shell. At $S = 95$ kN, further damage occurred at the vicinity of the supports due to shear deformation. However, this damage process zone did not lead to ultimate failure, due to the design of supports that enable *in-plane* rotation. It should be noted that without this measure, the damage induced by concentrated shear near the supports would become critical.

The numerically obtained load-deflection curves at the points P_1 to P_7 have been compared with the test results in Fig. 13 for load steps I and II. Considering load step I, the slope of the load-deflection branch is almost identical in the test and the simulation. Once the boundary conditions were changed by fixing the radial component of the supports and load step II was started, an increased structural stiffness was observed. The experimentally observed evolution of stiffness in load step II exhibits stiffening that can be ascribed to the nonlinear response of the elastomers at the supports. Because of the simplified representation in the numerical model using linear springs, this effect could be reproduced. This inconsistency is more significant for measuring points P_1 and P_2, revealing certain imperfections in the shell geometry or reinforcement layout.

While the simulation results are symmetric with respect to the x- and y-directions, the measured load-deflection curves exhibit differences in both directions. In the y-direction, the measured tensile strains ε_{xx} at the back and

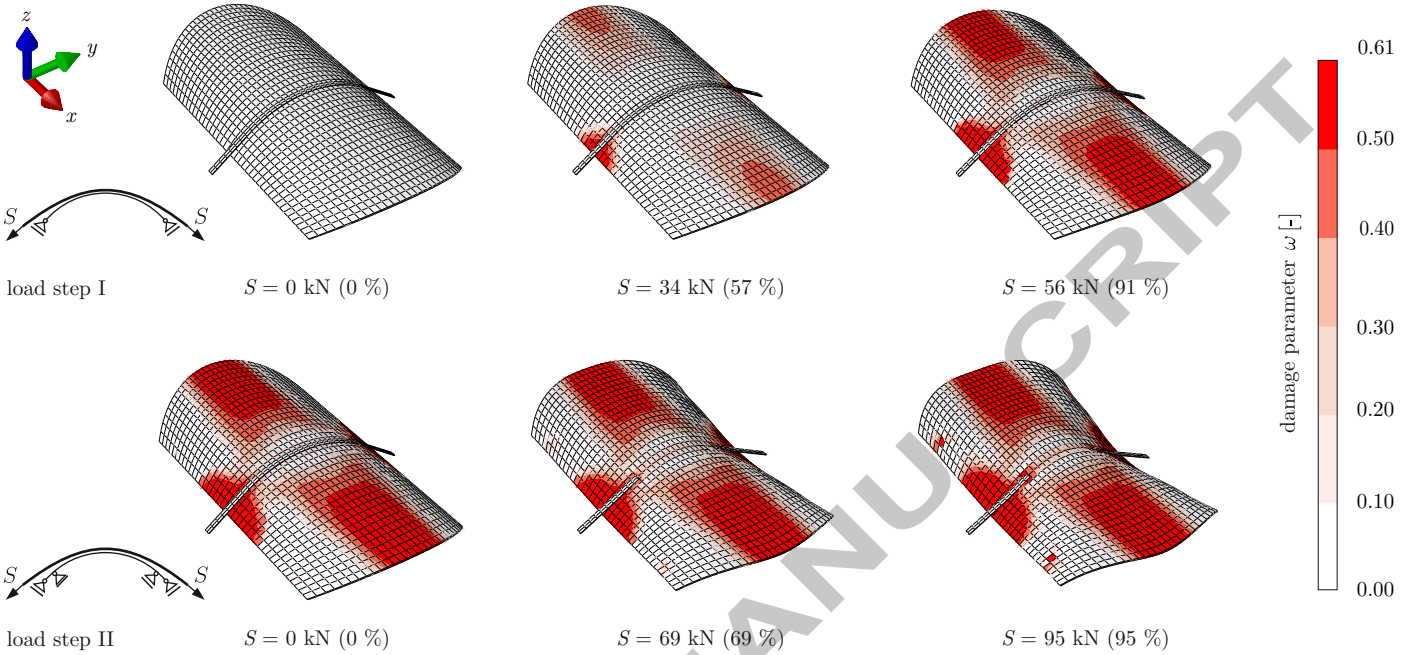

Figure 12: Evolution of damage during the load history

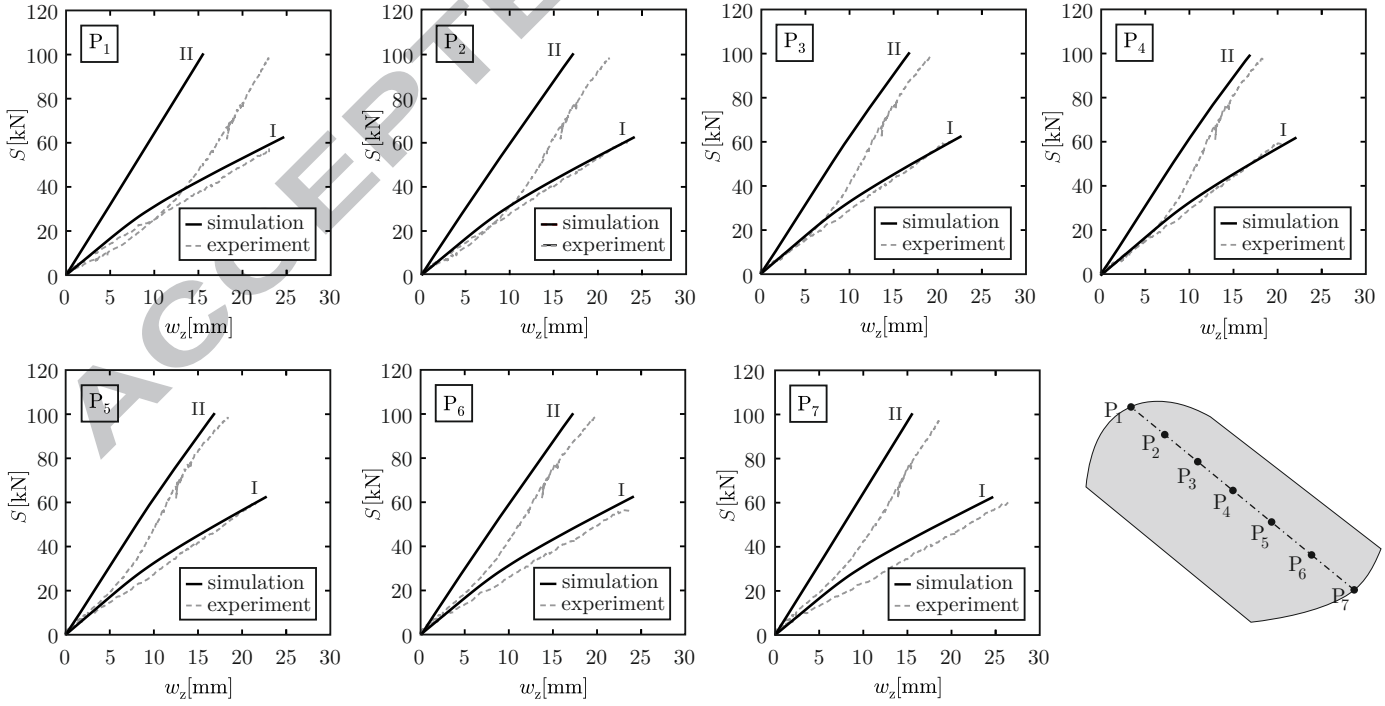

Figure 13: Load-deflection curves from test and simulation in z-direction for the measuring points P_1 to P_7

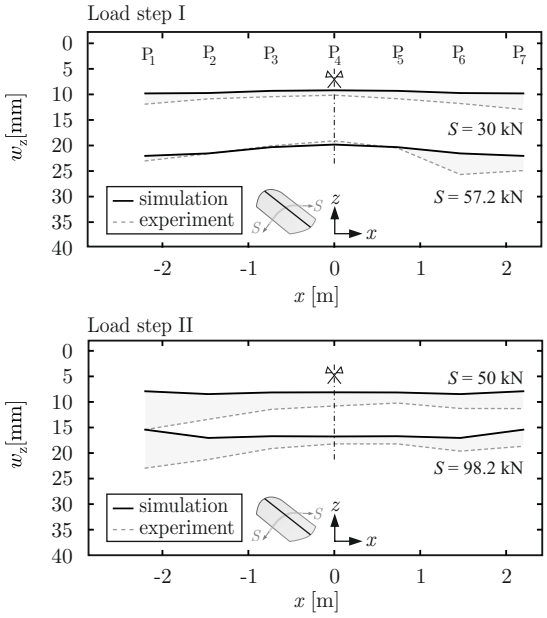

Figure 14: Vertical deflection of the barrel vault shell along its top line from test and simulation for the measuring points P_1 to P_7 in load steps I and II

front sides of the shell are not identical (Fig. 11). Further, the vertical deflection w_z at the point P_1 is larger than the vertical deflection at point P_7 (Fig. 13). To expose this lack of symmetry in the x-direction, the measured deflections at points P_1 to P_7 along the top line are compared with the simulation results in Fig. 14. The influence of geometric imperfections on the load-bearing capacity of TRC shell structures are beyond the scope of the present paper. A numerical study of the combined effect of material nonlinearity and geometric imperfections has been investigated by the authors in [37].

6. Comparison with the ULS design method

The performed experimental and numerical studies provide a unique chance to discuss the simplifications that are needed for generally applicable dimensioning approaches for TRC shells. Efficient limit state assessment for considering multiple load cases can only be based on linear structural analysis and superposition of the stress resultants. In case of the constructed bicycle stand (Fig. 1), such dimensioning and the safety assessment method has been described by the authors in [4, 5].

The first step of the proposed ULS assessment is to determine the values of cross-sectional strength for elementary loading configurations, i.e. in tension, bending, and in compression. The test specimens had the same cross sectional layout as the constructed shell (Fig. 5). Their mean values were evaluated as $n_{\mathrm{t,Rd}} = 476$ kN/m for tensile strength, $n_{\mathrm{c,Rm}} = 1360$ kN/m for compressive strength, and $m_{\mathrm{Rm}} = 3.3$ kNm/m for bending strength. The corresponding resistance envelope was constructed by connecting the three measured data points as shown in Fig. 15a. This simplified approximation is justified by the fact that the real envelope is nonlinear and provides significantly more cross-sectional resistance for interacting compression and bending. In case of combined tension and bending, the linear approximation has been justified using tests presented in [4].

In second step, the applied test load was considered as input of the ULS assessment procedure. The linear finite element calculation was performed with the boundary conditions corresponding to the test setup shown in Fig. 8. The reference load was represented by radial load $q_{\mathrm{ref}} = 10$ kN/m, corresponding to the force $S_{\mathrm{ref}} = R{\cdot}q_{\mathrm{ref}} = 14$ kN in the steel strip. The calculated stress resultants, i.e. the moments and the normal forces, were used to calculate the utilization ratio $\eta_{\mathrm{nm}} = \max(\eta_{\mathrm{nt}}, \eta_{\mathrm{nc}}) + \eta_{\mathrm{m}}$, representing the relative distance to the failure envelope. The values of η_{nm} are shown in the $n \times m$ interaction diagram in Fig. 15b for all integration points of the used finite element discretization. Apparently, at this configuration, the shall exhibits almost no bending moments. The spatial distribution of η_{nm} is depicted in Fig. 16.

The critical cross section exhibited the maximum level of utilization, $\eta_{\mathrm{nm,ref}} = 0.227$. This means that the ultimate load at full utilization, $\eta_{\mathrm{nm,el}} = 1.0$, would be attained for a load increased by the factor of $1/0.227$. Thus, the ultimate failure predicted using the applied ULS assessment method was

$$S_{\mathrm{el}} = S_{\mathrm{ref}}/\eta_{\mathrm{nm,ref}} = 14/0.227 = 61.7 \text{ kN}.$$

The ultimate load level predicted with the nonlinear simulation and confirmed in the test was $S_{\mathrm{test}} = 98.4$ kN. Thus, comparing the measured ultimate load with the evaluation using the linear design model

$$S_{\mathrm{test}}/S_{\mathrm{el}} = 98.4 \text{ kN}/61.7 \text{ kN} = 1.59$$

reveals 59% of structural redundancy with respect to the ULS assessment for the load case at hand.

The reason for higher value of ultimate stress can be seen in the stress redistribution owing to the crack pattern propagation depicted in Fig. 10b. The finely distributed cracks covered large zones of the shell that propagated from the critical cross sections at the middle of the longitudinal edges. This behavior leads to the activation of a larger effective area of reinforcement than assumed by the ULS assessment, that considers the state only in a single material point near the shell edge.

Even though this observation might be obvious, we consider it important to mention this quantitative relation between the nonlinear analysis and the ULS design method proposed for everyday engineering practice. The mechanisms of the stress redistribution in a composite consisting solely of brittle material components are owing to matrix cracking and debonding. The performed analysis quantifies the amount of stress redistribution capacity that can be mobilized by cracking and debonding between cracks

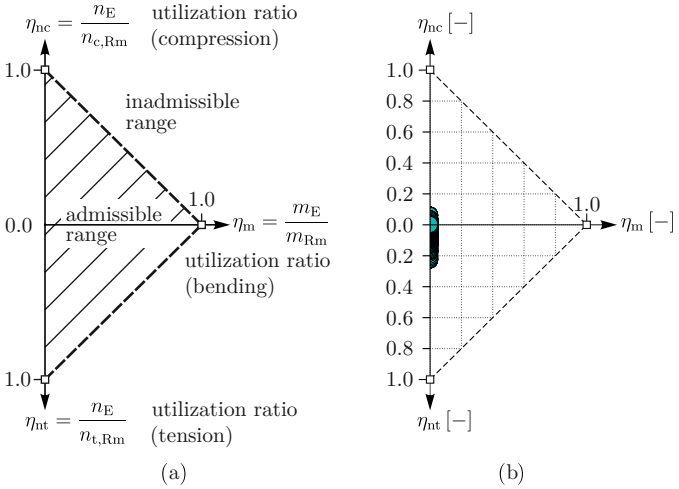

Figure 15: (a) dimensioning approach for TRC shell structures based on the normalized n-m interaction diagram; (b) computer-based evaluation of the utilization ratios for all elements and reference load $q_{ref} = 10$ kN/m

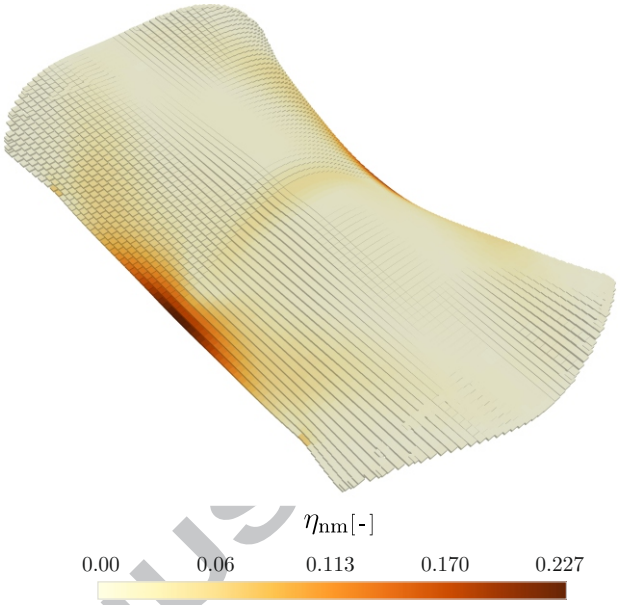

Figure 16: Utilization ratio of the TRC shell for the load imposed in the full-size test based on the mean values of the strength characteristics

for the provided shell geometry and for the considered load case. As a case study, it represents a contribution to the ongoing discussions on the development of design codes for TRC applications in the engineering research community.

7. Summary and conclusion

The goal in designing TRC shell structures is to utilize their high strength, as well as their ductility due to the interplay between the strain-hardening material behavior and the stress redistribution over large zones of the shell. Effective modeling support that can contribute to achieving this goal has been presented in this paper, along with a full-scale test of a vault shell serving as a roof structure over a bicycle stand.

In particular, the material model developed by the authors for analysis of thin-walled TRC shells reinforced with layers of textile fabrics has been applied for a thorough analysis of the shell behavior. The applied anisotropic damage model with strain-hardening was calibrated for the shell cross-sectional layout. Comparing the prediction with the test results proves the ability of the model to capture significant aspects of the shells structural behavior, including the evolution of damage due to cracking and the load-bearing capacity. Slight differences between the test results and the simulation were observed due to the imperfections in the shell geometry, which induced non-symmetric deformations. This fact calls for further studies on the sensitivity of the structural behavior and load-bearing capacity with respect to geometric imperfections in construction.

The test setup described in this paper was designed with the aim of exploring the structural behavior with high degree of stress redistribution and damage propagation throughout the shell. Therefore, the local failure of a cross section due to high local bending moments or local shear failure near the supports had to be avoided. The nonlinear analysis and the test results were used to quantify the structural redundancy involved in ultimate limit state design based on linear elastic structural analysis.

Acknowledgements

Financial support from *Deutsche Forschungsgemeinschaft (DFG)* (Project No. 276/2-2) is gratefully acknowledged.

References

[1] Ruhnau D. Hauchdünn, Beton im Besonderen: Pavillon aus Textilbeton an der RWTH Aachen. *Deutsche Bauzeitung*, 10:74–77, October 2015.

[2] Scholzen A., Chudoba R., and Hegger J. Thin-walled shell structure made of Textile Reinforced Concrete; Part I: structural design and construction. *Structural Concrete*, 16:106–114, 2015.

[3] Scholzen A., Chudoba R., and Hegger J. Thin-walled shell structure made of Textile Reinforced Concrete; Part II: experimental characterization, ultimate limit state assessment and numerical simulation. *Structural Concrete*, 16:115–124, 2015.

[4] Scholzen A., Chudoba R., and Hegger J. Ultimate limit state assessment of TRC structures with combined normal and bending loading. In Brameshuber W., editor, *11th International Symposium on Ferrocement (FERRO-11) and 3rd International Conference on Textile Reinforced Concrete (ICTRC-3)*, pages 159–166. RILEM Publications S.A.R.L., June 2015.

[5] Scholzen A., Chudoba R., Hegger J., and Will N. Light-weight precast shell elements made of textile reinforced concrete: production, experimental investigations and application potential. *Beton- und Stahlbetonbau*, 111(10):663–675, 2016.

[6] Cuypers H. and Wastiels J. A stochastic cracking theory for the introduction of matrix multiple cracking in textile reinforced concrete under tensile loading. In Hegger J., Brameshu-

ber W., and Will N., editors, *1st International RILEM Symposium*, pages 193–202. RILEM Publications S.A.R.L., September 2006.

[7] Mobasher B., Peled A., and Pahilajani J. Distributed cracking and stiffness degradation in fabric-cement composites. *Materials and Structures*, 39(3):317–331, June 2006.

[8] Larrinaga P., Chastre C., San-José J. T., and Garmendia L. Non-linear analytical model of composites based on basalt textile reinforced mortar under uniaxial tension. *Composites Part B: Engineering*, 55:518–527, 2013.

[9] Richter M. and Zastrau B. W. On the nonlinear elastic properties of textile reinforced concrete under tensile loading including damage and cracking. *Materials Science and Engineering: A*, 422(1-2):278–284, April 2006.

[10] Li Y., Chudoba R., Sadílek V., Rypl R., and Vořechovský M. Analysis of the tensile response of Textile Reinforced Concrete using digital image correlation technique combined with multiscale stochastic modelling. In Brameshuber W., editor, *11th International Symposium on Ferrocement (FERRO-11) and 3rd International Conference on Textile Reinforced Concrete (ICTRC-3)*, pages 141–148. RILEM Publications S.A.R.L., June 2015.

[11] Rypl R., Chudoba R., Scholzen A., and Vořechovský M. Brittle matrix composites with heterogeneous reinforcement: Multiscale model of a crack bridge with rigid matrix. *Composites Science and Technology*, 89:98 – 109, 2013.

[12] Barhum R. and Mechtcherine V. Effect of short, dispersed glass and carbon fibres on the behavior of textile-reinforced concrete under tensile loading. *Engineering Fracture Mechanics*, 92:56–71, September 2012.

[13] Hinzen M. and Brameshuber W. Load-bearing behaviour of Textile Reinforced Concrete with short fibres. In Barros Joaquim A.O., editor, *8th RILEM International Symposium on Fiber Reinforced Concrete: challenges and opportunities (BEFIB 2012)*, pages 254–266. RILEM Publications S.A.R.L., September 2012.

[14] Contamine R., Si Larbi A., and Hamelin P. Contribution to direct tensile testing of Textile Reinforced Concrete (TRC) composites. *Materials Science and Engineering: A*, 528(29-30):8589–8598, November 2011.

[15] Hartig J., Jesse F., Schicktanz K., and Häußler-Combe U. Influence of experimental setups on the apparent uniaxial tensile load-bearing capacity of Textile Reinforced Concrete specimens. *Materials and Structures*, 45(3):433–446, March 2012.

[16] Colombo I. G., Magri A., Zani G., Colombo M., and di Prisco M. Textile Reinforced Concrete: experimental investigation on design parameters. *Materials and Structures*, 46(11):1933–1951, November 2013.

[17] RILEM Technical Committee 232-TDT (Wolfgang Brameshuber). Recommendation of RILEM TC 232-TDT: test methods and design of textile reinforced concrete: Uniaxial tensile test: test method to determine the load bearing behavior of tensile specimens made of textile reinforced concrete. *Materials and Structures*, 49(12):4923–4927, December 2016.

[18] Hegger J., Will N., Bruckermann O., and Voss S. Load–bearing behaviour and simulation of textile reinforced concrete. *Materials and Structures*, 39(8):765–776, 2006.

[19] Graf W., Hoffmann A., Möller B., Sickert J., and Steinigen F. Analysis of textile-reinforced concrete structures under consideration of non-traditional uncertainty models. *Engineering Structures*, 29(12):3420–3431, 2007.

[20] Holler S., Butenweg C., Noh S. Y., and Meskouris K. Computational model of Textile-Reinforced Concrete structures. *Computers & Structures*, 82(23-26):1971–1979, September 2004.

[21] Bažant Z. P. and Planas J. *Fracture and Size Effect in Concrete and Other Quasibrittle Materials*. CRC Press, 1st edition, December 1997.

[22] Hofstetter G. and Mang H. *Computational Mechanics of Reinforced Concrete Structures*. Vieweg+Teubner Verlag, January 1995.

[23] Krätzig W. B. and Pölling R. An elasto-plastic damage model for reinforced concrete with minimum number of material parameters. *Computers and Structures*, 82(1516):1201–1215, 2004.

[24] Noh S. Y., Krätzig W. B., and Meskouris K. Numerical simulation of serviceability, damage evolution and failure of reinforced concrete shells. *Computers and Structures*, 81(811):843–857, 2003. K.J Bathe 60th Anniversary Issue.

[25] Jun D., Petryna Y., Bockhold J., and Stangenberg F. A rational framework for damage analyses of concrete shells. In K.J. Bathe, editor, *Computational Fluid and Solid Mechanics 2003*, pages 356–359. Elsevier Science Ltd, Oxford, 2003.

[26] Gericke O., Neuhäuser S., Mittelstädt J., and Sobek W. Computational evaluation of the load-bearing behaviour of segmented shell structures. In *Future Visions Proceedings of the International Association for Shell and Spatial Structures (IASS) Symposium*. KIVI (published on USB stick), August 2015.

[27] Waimer F., La Magna R., and Knippers J. Integrative numerical techniques for fibre reinforced polymers - forming process and analysis of differentiated anisotropy. *Journal of the International Association for Shell and Spatial Structures*, 54:301–309, 2013.

[28] Rajashekhar M. and Ellingwood B. Reliability of reinforced-concrete cylindrical shells. *Journal of Structural Engineering*, 121(2):336–347, February 1995.

[29] Soranakom C. and Mobasher B. Flexural analysis and design of Textile Reinforced Concrete. *Textilbeton Theorie und Praxis : Tagungsband zum 4. Kolloquium zu Textilbewehrten Tragwerken (CTRS4) und zur 1. Anwendertagung, Dresden, Germany*, pages 273–288, June 2009.

[30] Noh H. C. Nonlinear behavior and ultimate load bearing capacity of reinforced concrete natural draught cooling tower shell. *Engineering Structures*, 28(3):399–410, 2006".

[31] Bockhold J. and Petryna Y.S. Creep influence on buckling resistance of reinforced concrete shells. *Computers and Structures*, 86(78):702–713, 2008.

[32] Tysmans T., Adriaenssens S., Cuypers H., and Wastiels J. Structural analysis of small span Textile Reinforced Concrete shells with double curvature. *Composites Science and Technology*, 69(11-12):1790–1796, September 2009.

[33] Verwimp E., Tysmans T., Mollaert M., and Wozniak M. Prediction of the buckling behaviour of thin cement composite shells: Parameter study. *Thin-Walled Structures*, 108:20–29, 2016.

[34] Verwimp E., Tysmans T., Mollaert M., and Berg S. Experimental and numerical buckling analysis of a thin TRC dome. *Thin-Walled Structures*, 94:89–97, September 2015.

[35] Tomás A. and Tovar J. P. The influence of initial geometric imperfections on the buckling load of single and double curvature concrete shells. *Computers and Structures*, 96-97:34–45, April 2012.

[36] Reitinger R. and Ramm E. Buckling and imperfection sensitivity in the optimization of shell structures. *Thin-Walled Structures*, 23(14):159 – 177, 1995. Buckling Strength of Imperfection-sensitive Shells.

[37] Sharei E., Chudoba R., Scholzen A., and Hegger J. Thin-walled textile reinforced concrete shells:analysis of combined effect of anisotropic strain hardening and imperfect geometry. In Takeuchi T. Kawaguchi K., Ohsaki M., editor, *Spatial Structures in the 21st Century Proceedings of the International Association for Shell and Spatial Structures (IASS) Symposium*. published on USB stick, September 2016.

[38] Chudoba R., Sharei E., and Scholzen A. A strain-hardening microplane damage model for thin-walled textile-reinforced concrete shells, calibration procedure, and experimental validation. *Composite Structures*, 152:913–928, 2016.

[39] Jirásek M. Comments on microplane theory. *Mechanics of Quasibrittle Materials and Structures, Hermes Science Publications*, pages 55–77, 1999.

[40] Chudoba R. and Scholzen A. Textile-reinforced concrete: Structural behavior. In Triantafillou T., editor, *Textile Fibre Composites in Civil Engineering, 1st Edition*. Woodhead Publishing, February 2016.

[41] Hughes B. P. and Ash J. E. Anisotropy and failure criteria for concrete. *Matériaux et Construction*, 3(6):371–374, November 1970.

[42] Bažant Z. P. and Prat P. C. Microplane model for brittle-plastic material: I. Theory. *Journal of Engineering Mechanics*, 114(10):1672–1688, 1988.

[43] Dassault Systèmes Simulia Corp., Providence, RI, USA. *ABAQUS Analysis Users Manual, Volume IV: Elements, Version 6.11*, 2011.

[44] Sharei E., Chudoba R., and Scholzen A. Cross-sectional failure criterion combined with strain-hardening damage model for simulation of thin-walled textile-reinforced concrete shells. In Papadrakakis M., Papadopoulos V., Stefanou G., and Plevris V., editors, *ECCOMAS Congress 2016 - VII European Congress on Computational Methods in Applied Sciences and Engineering*, volume 4, pages 6823–6831. National Technical University of Athens (NTUA), June 2016.